

Ligand Replacement Approach to Raman-Responded Molecularly Imprinted Monolayer for Rapid Determination of Penicilloic Acid in Penicillin

Liyang Zhang,^{†,‡} Yang Jin,^{†,‡} Xiaoyan Huang,[†] Yujie Zhou,[†] Shuhu Du,^{*,†} and Zhongping Zhang^{‡,§}

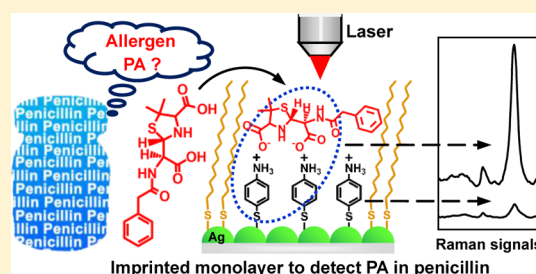
[†]School of Pharmacy, Nanjing Medical University, Nanjing, Jiangsu 211166, China

[‡]Institute of Intelligent Machines, Chinese Academy of Sciences, Hefei, Anhui 230031, China

[§]State Key Laboratory of Transducer Technology, Chinese Academy of Sciences, Hefei, Anhui 230031, China

Supporting Information

ABSTRACT: Penicilloic acid (PA) is a degraded byproduct of penicillin and often causes fatal allergies to humans, but its rapid detection in penicillin drugs remains a challenge due to its similarity to the mother structure of penicillin. Here, we reported a ligand-replaced molecularly imprinted monolayer strategy on a surface-enhanced Raman scattering (SERS) substrate for the specific recognition and rapid detection of Raman-inactive PA in penicillin. The bis(phenylenediamine)-Cu²⁺-PA complex was first synthesized and stabilized onto the surface of silver nanoparticle film that was fabricated by a bromide ion-added silver mirror reaction. A molecularly imprinted monolayer was formed by the further modification of alkanethiol around the stabilized complex on the Ag film substrate, and the imprinted recognition site was then created by the replacement of the complex template with Raman-active probe molecule *p*-aminothiophenol. When PA rebound into the imprinted site in the alkanethiol monolayer, the SERS signal of *p*-aminothiophenol exhibited remarkable enhancement with a detection limit of 0.10 nM. The imprinted monolayer can efficiently exclude the interference of penicillin and thus provides a selective determination of 0.10‰ (w/w) PA in penicillin, which is about 1 order of magnitude lower than the prescribed residual amount of 1.0‰. The strategy reported here is simple, rapid and inexpensive compared to the traditional chromatography-based methods.



Surface-enhanced Raman scattering (SERS) spectroscopy is a well-established and highly sensitive technique for identification and detection of chemical and biological species with the advantages of unique spectroscopic fingerprint and nondestructive data acquisition.^{1,2} It has been recognized that electromagnetic (EM) and chemical enhancements are two mechanisms accounting for the SERS effect, and the EM mechanism is mainly responsible for the occurrence of SERS.^{3,4} For this reason, the development of metal nano-particle-based SERS substrates to generate the enhanced Raman scattering signals has attracted considerable research interest. Currently, most studies are devoted to synthesizing various metal nanoparticles (NPs) (e.g., Au NPs and Ag NPs) that are then immobilized onto a glass slide or silicon wafer.^{5–9} Although metal nanoparticle substrates provide a new possibility for vibrational spectroscopy of a target molecule, the remarkable boost of the Raman intensity is usually observed on resonant dyes such as rhodamine-6G and crystal violet.¹⁰ The visible chromophores of resonant dyes may provide 2–3 orders of magnitude of additional enhancement relative to EM enhancement alone.^{11,12} However, most interesting analytes including drugs, pesticides and heavy metal ions have much smaller scattering cross sections than resonant dyes, and thus are Raman-inactive to exhibit the extremely weak response even

if enhanced. Alternatively, the molecular interactions by hydrogen bond, charge-transfer reaction and complexing coordination have widely been explored to amplify the Raman signals of a preresonant molecule,^{13–16} which may open a new avenue to the detection of Raman-inactive analytes. Disadvantageously, the interaction-based preresonance is easily affected by similar molecules, media or environments. Therefore, the SERS assays of real samples still have to face with the unsolved problems in selectivity, sensitivity and reliability.

Molecular imprinting is a convenient and powerful technique for the creation of specific recognition sites in synthetic polymers by using template molecules and functionalized monomers.^{17–20} The recognition cavities formed by the removal of templates are complementary to the size, shape and functionality of target molecules to provide the capability that selectively rebinds the targets over the structure-like compounds. However, the traditional imprinted materials suffer from the slow diffusion speed and low rebinding kinetics to targets due to the highly cross-linked rigid polymer network.^{21,22} Together with these disadvantages, the lack of signal

Received: August 11, 2015

Accepted: November 6, 2015

Published: November 6, 2015

response intrinsically limits the employment of an imprinting technique in chemical or biological sensors. An effective method to overcome these above difficulties is the recently developed surface molecular imprinting^{23–25} to locate the recognition sites on the surface of a polymer layer or other substrate, which greatly reduces the obstruction of molecular diffusion and accelerates the kinetics of rebinding. Surface imprinting has successfully been used in the recognition and separation of protein,²⁶ peptide,²⁷ cell,²⁸ bacteria,²⁹ etc. In particular, the fabrication of a surface imprinting monolayer on an optical/electrical device can offer the qualitative and quantitative measurements of a target by signal readout,^{30,31} driving the imprinting technique into a wide range of applications in chemical/biological sensors.

In the present work, we combined the SERS and surface imprinting together to develop a novel ligand-replaced molecularly imprinted monolayer (MIM) strategy for the rapid determination of penicilloic acid (PA) that is the serious allergen in penicillin.³² Different from the previously reported surface molecular imprinting chemosensory approaches,^{28,30} the as-synthesized bis(phenylenediamine)-Cu²⁺-PA (PPD₂-Cu²⁺-PA) as a template was imprinted into a monolayer of alkanethiol molecules on a piece of Ag nanoparticle film (Ag NF), and then the ligand phenylenediamine (PPD) was replaced by the structure-like Raman-active probe *p*-aminothiophenol (*p*-ATP). The fast rebinding of PA into the imprinted monolayer brought about the remarkable enhancement of Raman signal of the probe by the protonation of *p*-ATP via an acid–base pairing reaction. The molecularly imprinted SERS substrate exhibits a rapid Raman response and high sensitivity and thus can be potentially exploited for the identification of the allergen in penicillin drugs with complicated matrixes.

EXPERIMENTAL SECTION

Chemicals and Materials. Silver nitrate (AgNO₃), copper(II) nitrate trihydrate (Cu(NO₃)₂·3H₂O), tin(II) chloride dihydrate (SnCl₂·2H₂O), D-(+)-glucose, potassium bromide (KBr), sodium hydroxide (NaOH), ammonium hydroxide and ethanol were purchased from Sinopharm Chemical Reagent Co., Ltd. (Shanghai, China). *p*-Phenylenediamine (PPD) was supplied by Aladdin reagent Co., Ltd. (Shanghai, China). 1-Hexadecanethiol and *p*-aminothiophenol (*p*-ATP) were obtained from Sigma-Aldrich (St. Louis, USA). All of these reagents were of analytical grade and used as received without further treatment. Benzylpenicillin sodium and carbenicillin disodium were gifts from Shijiazhuang Pharmaceutical Group Co., Ltd. (Shijiazhuang, China). Penicilloic acid (PA) was prepared by alkaline hydrolysis of benzylpenicillin sodium according the reported literature.³³ Dialysis tubing with a molecular weight cutoff (MWCO) of 500 Da was from Spectrum Laboratories (Houston, USA).

Preparation of Ag NF on Glass Slide. Uniform Ag NF on a glass slide was prepared by a Br⁻-added silver mirror reaction. First, the glass slide was pretreated with piranha solution (98% H₂SO₄ and 30% H₂O₂ in ratio of 3:1, v/v) at 90 °C for 30 min to derive a hydroxyl surface. *Caution: piranha solution is aggressive and explosive. Never mix piranha waste with solvents. Check the safety precautions before using it.* After thorough rinsing with ultrapure water, the wet slide was successively immersed in the freshly prepared 0.2% SnCl₂ aqueous/ethanol solution (1:1, v/v) and 50 mM silver nitrate solution for 30 min. The [Ag(NH₃)₂]OH solution was prepared as follows: 20 mL of 50

mM silver nitrate was mixed with 0.2 mL of 1 M NaOH to form a brown precipitate, and then 240 μL of ammonium hydroxide was dropped until the precipitate completely dissolved to form the [Ag(NH₃)₂]OH solution. The solution was sequentially mixed with 3 mL of 0.2 M KBr and 1.25 mL of 1 M glucose under stirring. After that, the pretreated glass slide was swiftly dipped into the above mixture solution and left for 40 min at 20 °C. Finally, resultant Ag NF on a glass slide was rinsed several times with distilled water and stored in N₂-saturated ultrapure water for further use. Meanwhile, the classical Ag NF on a glass slide was also prepared with the same procedure but without the addition of KBr.

Formation of Complex Template. The complex template PPD₂-Cu²⁺-PA was formed by a two-step coordination method. Briefly, 10 mL of 1.0 × 10⁻³ M PPD was mixed with an isometric solution of 5.0 × 10⁻⁵ M Cu(NO₃)₂ under stirring. After reaction for 1 h, 250 μL of 1.0 × 10⁻² M PA was added to the above solution and the mixture was stirred for another 1 h at room temperature. The PPD₂-Cu²⁺-PA solution was finally purified by dialysis for 24 h.

PA-Imprinted Monolayer on Ag NF. First, the Ag NF slide was soaked in PPD₂-Cu²⁺-PA solution for 2 h and rinsed with ultrapure water. Then, the Ag NF slide with the preadsorbed complex templates was immersed in 5.0 × 10⁻⁴ M hexadecanethiol for another 4 h, resulting in the formation of a self-assembled monolayer around the complex template on the surface of Ag NF. Subsequently, the complex templates were removed by elution of aqueous NaOH (pH 11.0). Finally, the Ag NF slide with the alkanethiol monolayer was further incubated in 1.0 × 10⁻⁶ M *p*-ATP for 8 h to anchor SERS probes in the imprinted cavity. After the excessive *p*-ATP on the Ag NF was removed by washing with ethanol, the MIM on Ag NF was obtained. Meanwhile, the nonimprinted monolayer (NIM) on Ag NF was also prepared in the absence of complex templates.

SERS Mapping on Ag NF. The prepared Ag NF was immersed in 1.0 × 10⁻⁵ M *p*-ATP solution for 1 h and then the surface was mapped with the Raman band of *p*-ATP at 1072 cm⁻¹. All SERS mapping data were obtained by using a 633 nm laser with 8 mW power and 10× objective. The collecting time was 2 s with 2 rounds of accumulations and the pinhole aperture was 25 μm. The mapping area was 40 × 40 μm² with a step size of 8 μm. In all, 25 Raman spectra were collected for each map.

SERS Detection of PA in Spiked Penicillin. Typically, PA with different amounts was first spiked into penicillin, and the mixture was dissolved into 50 mL of ultrapure water. Prior to the assay, the sample was diluted 10 000 times with ultrapure water. Then, 10 μL of sample solution was dropped onto the molecularly imprinted SERS substrate. The Raman spectra were recorded using a 633 nm laser with 8 mW power and 10× objective. The collecting time was 5 s with 4 rounds of accumulations and the pinhole aperture was 25 μm. The Raman spectra were the average of 5 scans. The accuracy of the method was further evaluated from the recovery test that was performed by adding the known amounts of reference PA in samples.

Characterizations and Instruments. The morphologies and structures of Ag NPs were examined by an S-3400N II scanning electron microscopy (SEM) instrument (Tokyo, Japan). UV–vis absorption spectra were obtained by an UV-2501 spectrometer (Tokyo, Japan). Raman measurements were conducted with Thermo Fisher DXR Raman Microscope

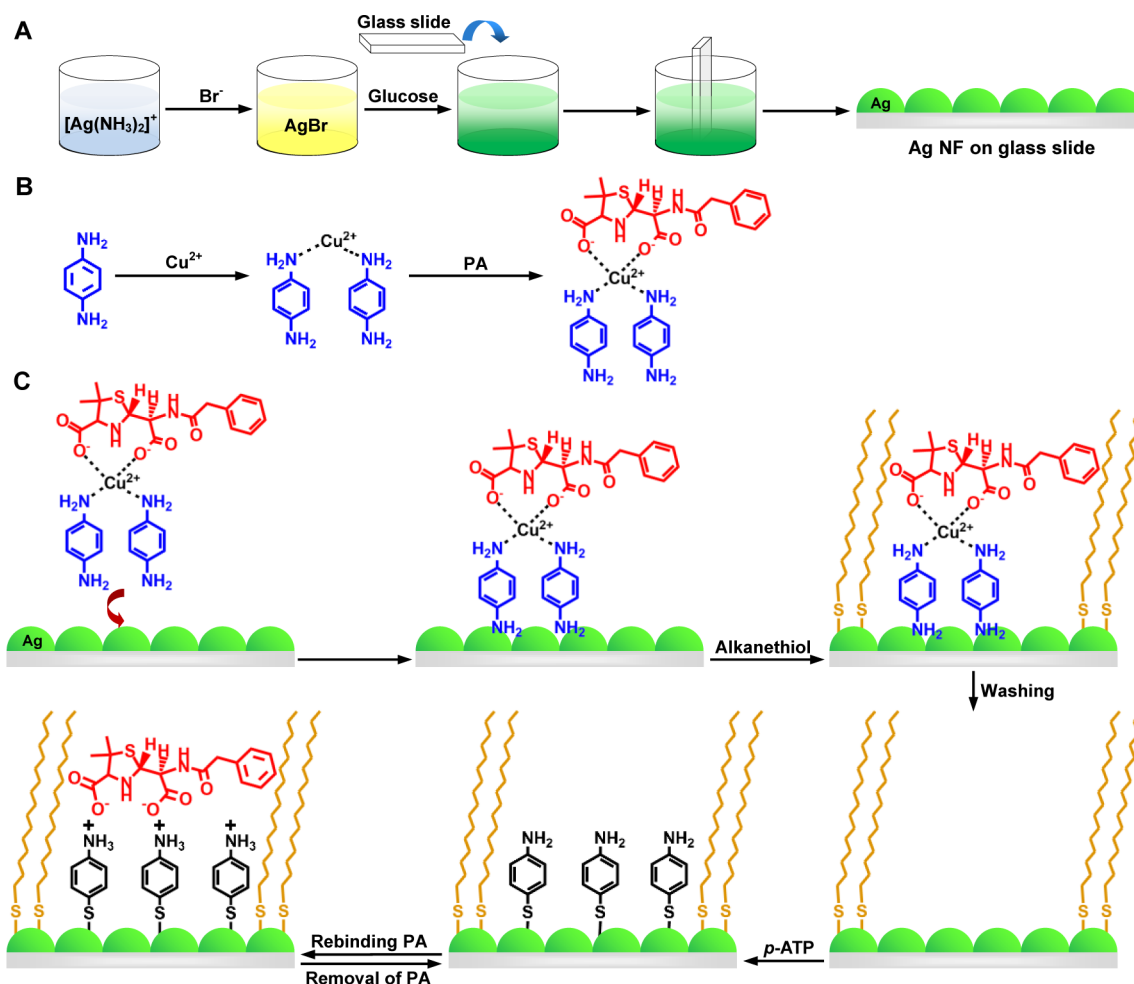


Figure 1. Schematic illustrations for (A) the preparation of Ag NF through Br^- -added silver mirror reaction, (B) the formation of complex template and (C) the imprinting procedure of PA on Ag NF.

(Madison, USA) equipped with a CCD detector in back-scattered configuration using a $10\times$ objective, and the He–Ne 633 nm laser was used as the excitation source. The structural identifications were performed using an Agilent 6410B Triple Quad LC-ESI-MS/MS instrument (MassHunter Data Acquisition, Santa Clara, USA).

RESULTS AND DISCUSSION

PA-Imprinted Monolayer on Ag NF. Noble metal Ag has been most frequently used as the enhancer of Raman spectra, and it yields a Raman enhancement 2 or 3 orders of magnitude higher than that of Au for the same particle size and shape.³⁴ In the current work, we attempt to combine the surface molecular imprinting at Ag film and the SERS property of Ag film together to achieve both the specific recognition and Raman response to PA analyte in penicillin. On the one hand, the formation of MIM requires a highly flat/uniform and large-area Ag film for the regular arrangement of the alkanethiol monolayer. On the other hand, the Ag film should consist of Ag NPs with a size of 40–50 nm to obtain excellent Raman enhancement.³⁵ As well-known, the classical silver mirror reaction has been widely used in the fabrication of highly uniform/dense Ag film. Here, a Br^- -added silver mirror reaction is used to prepare the Ag NF to meet the requirements of molecular imprinting and SERS effect. As shown in Figure 1A, Br^- ions are added into the $[\text{Ag}(\text{NH}_3)_2]\text{OH}$ solution to

slow down the reduction rate of $[\text{Ag}(\text{NH}_3)_2]^+$ by the formation of AgBr , leading to the large-scale growth of Ag NPs on the glass slide.

A ligand replacement strategy is developed to fabricate the MIM substrate for the SERS detection of PA. First, the complex template is synthesized by the coordination reaction of two PPD molecules and one PA molecule with one Cu^{2+} ion because a PA molecule contains two carboxyl groups (Figure 1B). The free amino group of PPD can adsorb onto the surface of Ag NF due to the interaction between the lone electron pair of the amino group and Ag NPs. As shown in Figure 1C, after the $\text{PPD}_2\text{-Cu}^{2+}\text{-PA}$ is adsorbed onto the Ag NF slide is immersed in the hexadecanethiol solution to obtain the alkanethiol monolayer on the Ag NF by the formation of a Ag–S bond. Thus, the $\text{PPD}_2\text{-Cu}^{2+}\text{-PA}$ template is stabilized in the alkanethiol monolayer. Subsequently, the $\text{PPD}_2\text{-Cu}^{2+}\text{-PA}$ template is decomposed by washing with strong basic NaOH, and the imprinted recognition site of PA is finally formed in the alkanethiol monolayer.

PA is a Raman-inactive molecule and exhibits very weak Raman signals if enhanced by Ag NPs. Here, we use an indirect Raman measurement for the detection of PA by the employment of a Raman-active probe. The Raman probe $p\text{-ATP}$ is modified in the imprinted cavity by the formation of a Ag–S bond (Figure 1C), which does not change the imprinting effect due to the similar structure of $p\text{-ATP}$ to PPD. It should

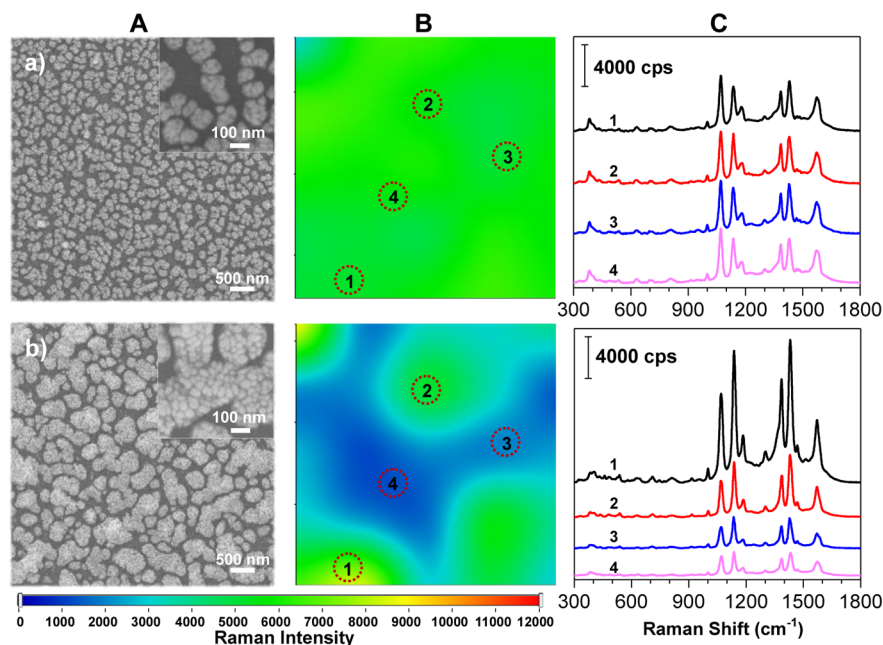


Figure 2. (A) SEM images of Ag films prepared by (a) the Br⁻-added method and (b) the classical silver mirror reaction. (B) SERS images mapped with the Raman band at 1072 cm⁻¹ after the two Ag NF substrates were immersed in 1.0 × 10⁻⁵ M *p*-ATP for 1 h. (The color bar indicates the Raman signal intensity.) (C) Corresponding Raman spectra at the indicated sites in panel B.

Table 1. CV for Different Types of Ag NF Substrates

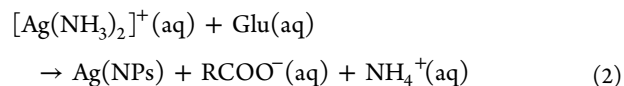
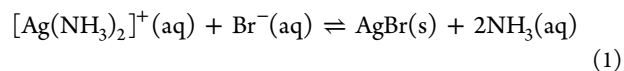
substrate type	intrasubstrate				intersubstrate			
	N_{intra}^a	avg ^b	SD ^c	CV (%) ^d	N_{inter}^e	avg	SD	CV (%)
Ag NF	25	5202.74	327.77	6.30	5	5214.67	505.30	9.69
classical Ag NF	25	3584.99	1962.44	54.7	5	4551.29	2057.18	45.2

^aThe number of Raman spectra collected for each substrate. ^bAverage Raman intensity of *p*-ATP at 1072 cm⁻¹ obtained from mapping data. ^cStandard deviation. ^dCV is defined as the SD divided by the mean intensity. ^eThe number of test substrate each with ten spectra.

be noted that the stability of a Ag–S bond is actually affected by the possible oxidation of the Ag surface. In the present work, a high concentration of hexadecanethiol was used, and a highly dense monolayer of alkanethiol with a long alkyl chain covered the surface of the Ag film, greatly reducing the possibility of oxidation of Ag NPs. Furthermore, the as-prepared alkanethiol monolayer on the Ag film was kept in nitrogen-saturated water to avoid the occurrence of oxidation reaction. These can ensure the stability of MIM before use. When PA rebinds into the recognition cavity of MIM by the acid–base interaction between carboxyl and amino groups, the SERS signal of *p*-ATP is obviously enhanced due to the polarization of the *p*-ATP molecule³⁶ by the protonation of its amino group, providing the detection of PA.

Structure and SERS Effect of Ag NF. In fact, our Br⁻-added method and the classical silver mirror reaction can produce highly dense Ag films without any difference by the observation of naked eye (Figure S1). However, the SEM images show that the aggregates of Ag NPs obtained by the Br⁻-added method are much smaller and more uniform than those by the classical silver mirror reaction, and the resultant surface of the Ag NF is more flat (Figure 2A, a and b). The inset images reveal the 40–50 nm Ag NPs in these aggregates to offer the effective Raman enhancement. The addition of Br⁻ can lead to the reversible transformation from [Ag(NH₃)₂]⁺ to the slightly soluble AgBr (eq 1), which also causes a cathodic shift of the reduction potential of [Ag(NH₃)₂]⁺/Ag.³⁷ These

greatly decrease the reduction rate of Ag(I) (eq 2), and thus the resultant Ag NPs aggregates become smaller and more uniform.



Moreover, SERS mappings were performed to compare the SERS effects of two Ag films. The two Ag films were separately immersed in 1.0 × 10⁻⁵ M *p*-ATP for 1 h, and then the surface was mapped with the Raman band 1072 cm⁻¹ of *p*-ATP. As shown in Figure 2B, the Raman intensity is highly uniform in the scanned region on the Ag NF (a) by the homogeneous color distribution. In contrast, the obvious fluctuation of Raman intensity on the Ag NF (b) is observed. Figure 1C shows that the Raman spectra of *p*-ATP at the randomly selected four sites of Ag NF (a) have identical intensities, whereas the intensities of four Raman spectra on the Ag NF (b) are completely different from each other. Table 1 lists the data of coefficients of variation (CV) for different points within the same Ag NF substrate (intrasubstrate) and among different Ag NF substrates (intersubstrate). These above results confirm the identical capabilities of Raman enhancements of different sites on Ag NF prepared by the Br⁻-added method.

Meanwhile, the enhancement sensitivity of Ag NF was also evaluated by adding different amounts of *p*-ATP onto the

surface of the Ag NF. The Ag NF (a) displays high Raman enhancement, which is nearly 4.8-fold that of Ag NF (b) (Figure S2). In addition, the Raman characteristic band of *p*-ATP at 1072 cm^{-1} can be clearly observed on the Ag NF (a) even when the concentration of *p*-ATP is reduced to 5.0×10^{-7} M (Figure S3). These measurements demonstrate that the as-prepared Ag NF (a) as SERS substrate exhibits excellent uniformity, reproducibility and sensitivity.

PPD₂-Cu²⁺-PA Template. Figure 3A shows the evolution of absorption spectra of PPD solution upon the titration with

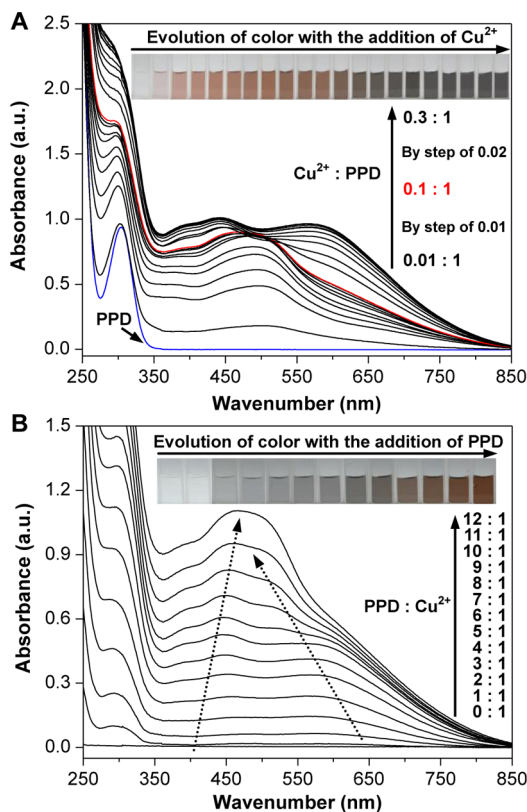


Figure 3. Evolution of UV-vis absorption spectra of (A) 1.0 mM PPD solution upon the addition of Cu^{2+} at the molar ratio ($\text{Cu}^{2+}/\text{PPD}$) from 0.01:1 to 0.3:1, and (B) 0.1 mM Cu^{2+} solution upon the addition of PPD at the molar ratio ($\text{PPD}/\text{Cu}^{2+}$) from 0:1 to 12:1. The inset images are the corresponding colors of the solutions.

Cu^{2+} . The aqueous PPD exhibits only one characteristic absorption band at 305 nm (blue curve in Figure 3A), whereas one new absorption band at 490 nm appears with the addition of Cu^{2+} and becomes stronger until the molar ratio of Cu^{2+} to PPD reaches 0.1:1 (the red curve in Figure 3A). Meanwhile, it can be observed that the solution changes from colorless to light brown to deep brown (the inset image). The mass spectroscopy gives a main peak at m/z : 280 $[\text{M} + 1]^+$ (Figure S4), indicating the presence of a bidentate coordination complex $[\text{Cu}(\text{PPD})_2]^{2+}$. With the further increase of Cu^{2+} , the single characteristic band gradually evolves into two split absorption bands at 440 and 590 nm, and the solution becomes gray and slightly turbid (the inset image), which is caused by the formation of a long-chain coordination complex (Figure S5).³⁸ Moreover, the result obtained from the titration of Cu^{2+} solution with PPD shows that the long-chain coordination complex can also transfer to the bidentate coordination

complex $[\text{Cu}(\text{PPD})_2]^{2+}$ by increasing the molar ratio ($\text{PPD}:\text{Cu}^{2+}$) to 10:1 (Figure 3B and the inset image).

To avoid the formation of a long-chain coordination complex, we used the molar ratio ($\text{PPD}:\text{Cu}^{2+}$) of 20:1 in the synthesis of the $\text{PPD}_2\text{-Cu}^{2+}\text{-PA}$ template. The Cu^{2+} ion in the $[\text{Cu}(\text{PPD})_2]^{2+}$ complex still has two additional coordination sites to bind PA by its two carboxyl groups, as illustrated in Figure 1B. Figure S6-A shows that the absorption intensity of characteristic band of $[\text{Cu}(\text{PPD})_2]^{2+}$ at 490 nm gradually decreases with the increase of PA concentration and finally keeps a constant intensity, accompanying a color change from dark red to light brown (the inset of Figure S6-A), and indicating the formation of the $\text{PPD}_2\text{-Cu}^{2+}\text{-PA}$ complex. When the molar ratio of $\text{PPD}:\text{Cu}^{2+}:\text{PA}$ is 20:1:5, a tetradentate coordination complex ($\text{PPD}_2\text{-Cu}^{2+}\text{-PA}$) is formed with a strong peak at m/z : 630 by LC-MS analysis (Figure S6-B).

Molecular Imprinting by Alkanethiol Monolayer. The imprinting of the $\text{PPD}_2\text{-Cu}^{2+}\text{-PA}$ template was carried out first by immersing the Ag NF into the $\text{PPD}_2\text{-Cu}^{2+}\text{-PA}$ solution, leading to the adsorption of $\text{PPD}_2\text{-Cu}^{2+}\text{-PA}$ at the surface of Ag NPs by the interaction between the amino group of PPD and Ag. Then, the Ag NF slide was immersed into the hexadecanethiol solution to form the alkanethiol monolayer around the $\text{PPD}_2\text{-Cu}^{2+}\text{-PA}$ templates. However, this is only an ideal situation because $\text{PPD}_2\text{-Cu}^{2+}\text{-PA}$ templates adsorbed at Ag NF may be replaced by hexadecanethiol molecules due to the formation of stronger Ag-S bonds between hexadecanethiol molecules and Ag NPs. As shown in Figure S7-A, the intensities of Raman signals of hexadecanethiol increase with the time and reach constant after 4 h. Meanwhile, the Raman intensity of PPD at 606 cm^{-1} is closely related to the concentration of hexadecanethiol (Figure S7-B). When the concentration of hexadecanethiol is larger than 5.0×10^{-4} M, the Raman intensity of PPD (at 606 cm^{-1}) obviously becomes weak. This reveals that a higher concentration of hexadecanethiol may make $\text{PPD}_2\text{-Cu}^{2+}\text{-PA}$ templates replaced by hexadecanethiol molecules, decreasing the molecularly imprinted effect. Therefore, 5.0×10^{-4} M hexadecanethiol is used for constructing a stably imprinted monolayer, in which more $\text{PPD}_2\text{-Cu}^{2+}\text{-PA}$ templates are reserved on the surface of the Ag NF, and the alkanethiol monolayer is also highly dense. Before the removal of the complex-template, the prepared substrate clearly exhibits the SERS signal of PPD (Figure S8).

Raman Enhancement Mechanism. After the removal of the $\text{PPD}_2\text{-Cu}^{2+}\text{-PA}$ template, the PA molecule can selectively enter the recognition cavity on the imprinted monolayer, but the SERS signal of PA is weak due to its small Raman cross section (Figure S9). In this work, we further modified the Raman-active *p*-ATP into the imprinted cavity, in which *p*-ATP has the similar shape and size to the PPD ligand, thus not changing the configuration of the recognition site (Figure 4A). When PA analyte enters the modified recognition site, two carboxyl groups of PA form the acid-base pairings with the free amino groups of *p*-ATP (Figure 4B). The protonation of amino groups leads to polarization of the *p*-ATP molecules and causes the huge Raman enhancement of the *p*-ATP probes, as shown by the Raman spectra in the right side of Figure 4. According to the mechanism, the acidic pH will also cause the Raman enhancement of the *p*-ATP molecule (Figures S10 and S11), and thus the use of the SERS substrate should be in the pH range of 6–8.

Sensitivity, Reliability and Selectivity for Detection of PA. Figure 5A shows the evolution of Raman spectra of *p*-ATP

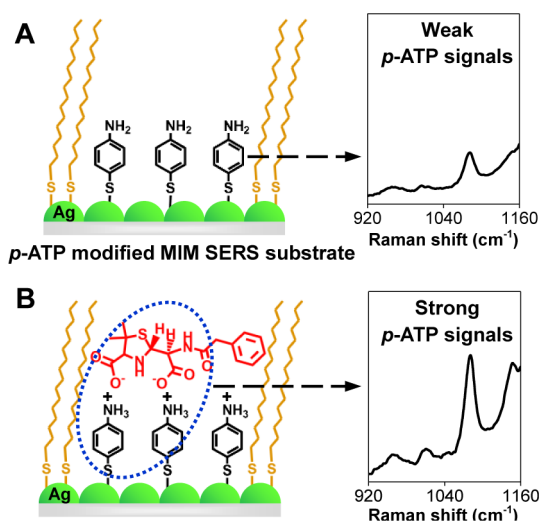


Figure 4. (A) *p*-ATP-modified MIM and its SERS response. (B) Working principle for SERS detection of PA on the MIM substrate.

modified in the imprinted cavity after the addition of PA onto the imprinted monolayer SERS substrate. The Raman spectrum of *p*-ATP gradually enhances with the increase of PA concentration from 1.0×10^{-10} to 5.0×10^{-8} M, indicating that PA can rebind into the recognition site and interact with the *p*-ATP probe, as shown in Figure 4B. The separate/sharp Raman peak at 1072 cm^{-1} (assigned to the stretching vibration of C–S) is selected as the quantitative evaluation of Raman enhancement. Clearly, the Raman intensity rapidly enhances with the concentration of PA and finally reaches the maximum at the concentration of 1.0×10^{-8} M (Figure 5B), which is 2.2-fold stronger than that of the blank substrate. Even with 0.1 nM PA, the Raman intensity is still enhanced by 19%, revealing a nano-molar-level sensitivity to PA. Meanwhile, Raman intensity increases in a linear fashion with respect to the PA concentrations ranging from 2.5×10^{-10} to 1.0×10^{-8} M with a good linear correlation coefficient $R^2 = 0.9825$ (inset of Figure 5B). The results suggest that PA can be quantitatively detected using the imprinted monolayer SERS substrate. Furthermore, the substrate can be cyclically used by washing off the bound PA with aqueous NaOH (pH 11) (Figure 5C).

To obtain a better understanding on the sensing mechanism, the selectivity was examined by the comparisons of MIM and NIM with the additions of two structural analogues (penicillin and carbenicillin) to PA. For the NIM, the additions of the three analytes only produce very weak Raman enhancements with the similar low intensities (Figure 6A). For the MIM, however, the Raman enhancements of *p*-ATP exhibit an obvious difference, in which the enhancements are 12.7-, 2.0- and 4.7-fold higher than those on the NIM with the identical additions of PA, penicillin and carbenicillin, respectively. That is to say, the imprinted sites formed by the alkanethiol monolayer have much higher selectivity in molecular structure to PA than that to penicillin/carbenicillin. Meanwhile, Figure 6A also shows the higher enhancement for the addition of carbenicillin than that of penicillin on the imprinted substrate. As given in the inset of Figure 6A, PA and carbenicillin molecules contain two carboxyl groups, while penicillin only contains one carboxyl group. The stronger acid–base interaction between the *p*-ATP and PA/carbenicillin results in the higher Raman enhancement. In addition, the similar experiments were carried out on the *p*-ATP modified Ag NF without the imprinted monolayer (Figure

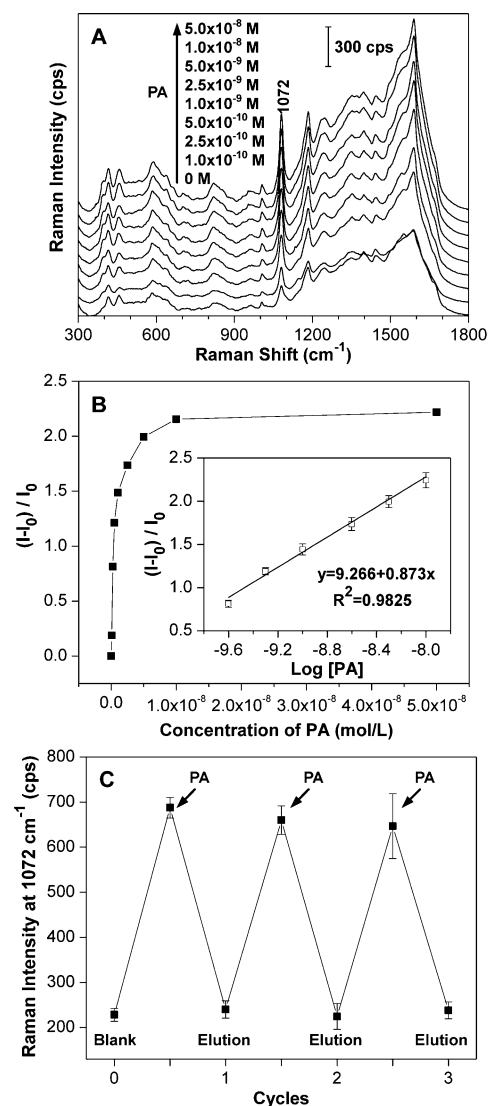


Figure 5. (A) Raman spectra of *p*-ATP after the addition of PA with different concentrations onto the imprinted monolayer SERS substrate. (B) Dependence of Raman enhancement of *p*-ATP on the concentration of PA. The inset is the linear correlation between the Raman enhancement of *p*-ATP and the logarithm of PA concentrations from 2.5×10^{-10} to 1.0×10^{-8} M. Here, I_0 and I are Raman intensities of *p*-ATP at 1072 cm^{-1} in the absence and presence of PA, respectively. (C) Cyclic detection of *p*-ATP Raman intensity at 1072 cm^{-1} by repeatedly adding $10 \mu\text{L}$ of 5.0×10^{-9} M PA solution on the SERS substrate.

S12). The additions of PA and analogous carbenicillin produced the similarly large Raman enhancements of *p*-ATP. These above results further confirm the selectivity of molecular imprinting and the mechanism of Raman enhancement as illustrated in Figure 4.

The high selectivity is mainly owing to the molecular size and shape recognition of the imprinted monolayer to the target molecule. From the steric configurations of the three molecules (Figure 6B), the β -lactam ring and thiazolidine ring in penicillin/carbenicillin link together to form a rigid nonplanar structure (the red zones), whereas the β -lactam ring in PA is opened to leave only a thiazolidine ring, leading to the large differences in steric structure between PA and penicillin/carbenicillin. Therefore, PA-imprinted cavities can offer a better

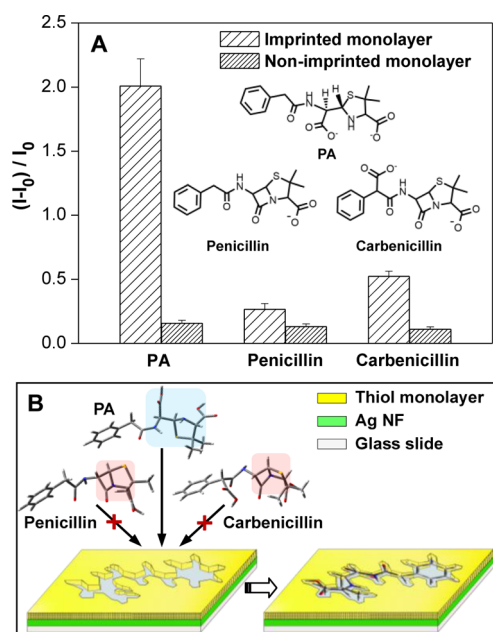


Figure 6. (A) Selectivity of the imprinted/nonimprinted monolayer for the determination of PA over other structural analogues with the concentration of 5.0×10^{-9} M. Here, I_0 and I are Raman intensities of *p*-ATP at 1072 cm^{-1} in the absence and presence of analytes, respectively. (B) Schematic diagram of the selectivity of imprinted monolayers toward PA compared with other structural analogues.

selectivity to PA than that to its analogues penicillin and carbenicillin.

Detection of PA in Spiked Penicillin. In the detection of a practical sample, we spiked 0.10 to 1.0 mg of PA in 1.0 g of penicillin, and then $10 \mu\text{L}$ of aqueous solution of the mixture was added onto the surface of the molecularly imprinted SERS substrate. With the increase of PA amount in penicillin, the characteristic vibrating band of *p*-ATP at 1072 cm^{-1} becomes stronger (Figure 7A). The limits of detection of PA residues in penicillin is about 0.10‰ (w/w), which is about 1 order of magnitude lower than that in previously reported results.³⁹ Meanwhile, the Raman enhancements versus the PA contents in penicillin can be illustrated by a fitting equation with $R^2 = 0.9894$ (Figure 7B). Furthermore, when three known amounts of PA are added in penicillin samples, the recoveries of PA in the spiked penicillin samples are in the range of 95.00%–102.50%, and the RSDs are in the range of 3.92%–5.34% (Table S1). These results confirm that the imprinted monolayer SERS substrate has a high reliability and accuracy to meet the requirements of the detections of real samples.

CONCLUSIONS

In summary, we have developed a ligand-replaced MIM strategy on the surface of Ag NF for the specific identification and rapid detection of trace PA in penicillin. It has been demonstrated that the Ag NF obtained from the Br^- -added silver mirror reaction exhibits excellent uniformity and high Raman enhancement. Importantly, a complex template between PA and PPD is successfully prepared by the chelation of Cu^{2+} , reducing the lateral diffusion of the alkanethiol monolayer and improving the stability of imprinted cavity, and subsequently replaced by the Raman-active probe molecule *p*-ATP. The formed MIM exhibits a better site accessible to the PA molecule with an excellent recognition selectivity. The

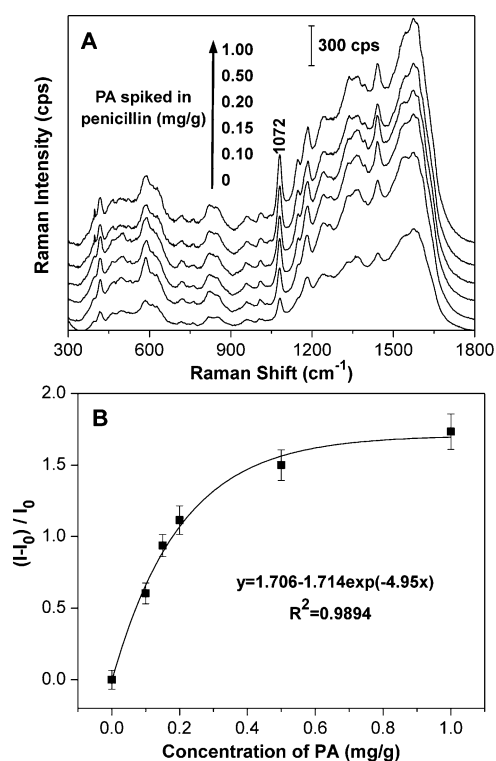


Figure 7. (A) Raman spectra of *p*-ATP after the addition of penicillin spiked with different amounts of PA onto the imprinted monolayer SERS substrate. (B) Plot of Raman enhancement as a function of PA concentrations from 0 to 1.0 mg/g in penicillin matrix. Here, I_0 and I are Raman intensities of *p*-ATP at 1072 cm^{-1} in the absence and presence of different concentrations of PA, respectively.

addition of PA analyte can remarkably enhance the SERS signal with a high sensitivity down to the nanomolar level. In particular, the imprinted monolayer SERS substrate can rapidly detect the PA residue in penicillin, and does not require any sophisticated sampling, beforehand separation/extraction and preconcentrated procedures. The method reported here may provide potential applications in the on-site and real-time monitoring of the allergen in penicillin drugs for their use securely.

ASSOCIATED CONTENT

Supporting Information

The Supporting Information is available free of charge on the ACS Publications website at DOI: 10.1021/acs.analchem.5b03088.

Additional information as noted in text (PDF).

AUTHOR INFORMATION

Corresponding Author

*S. Du. Tel./Fax: +86-25-86868476. E-mail: shuhudu@njmu.edu.cn.

Author Contributions

[†]These authors contributed equally.

Notes

The authors declare no competing financial interest.

ACKNOWLEDGMENTS

This work is supported by the National Natural Science Foundation of China (No. 21275075) and the Specialized

Research Fund for the Doctoral Program of Higher Education of China (No. 20113234110001).

(39) Zhang, L.; Jin, Y.; Mao, H.; Zheng, L.; Zhao, J.; Peng, Y.; Du, S.; Zhang, Z. *Biosens. Bioelectron.* **2014**, *58*, 165–171.

REFERENCES

- (1) Qian, X. M.; Nie, S. M. *Chem. Soc. Rev.* **2008**, *37*, 912–920.
- (2) Abbas, A.; Brimer, A.; Slocik, J. M.; Tian, L. M.; Naik, R. R.; Singamaneni, S. *Anal. Chem.* **2013**, *85*, 3977–3983.
- (3) Dasary, S. S. R.; Singh, A. K.; Senapati, D.; Yu, H.; Ray, T. P. C. *J. Am. Chem. Soc.* **2009**, *131*, 13806–13812.
- (4) Doering, W. E.; Nie, S. *J. Phys. Chem. B* **2002**, *106*, 311–317.
- (5) Liu, B. H.; Han, G. M.; Zhang, Z. P.; Liu, R. Y.; Jiang, C. L.; Wang, S. H.; Han, M. Y. *Anal. Chem.* **2012**, *84*, 255–261.
- (6) Yang, L.; Li, P.; Liu, J. *RSC Adv.* **2014**, *4*, 49635–49646.
- (7) Gao, C.; Hu, Y.; Wang, M.; Chi, M.; Yin, Y. *J. Am. Chem. Soc.* **2014**, *136*, 7474–7479.
- (8) Yang, X.; Gu, C.; Qian, F.; Li, Y.; Zhang, J. Z. *Anal. Chem.* **2011**, *83*, 5888–5894.
- (9) Liu, H.; Yang, Z.; Meng, L.; Sun, Y.; Wang, J.; Yang, L.; Liu, J.; Tian, Z. *J. Am. Chem. Soc.* **2014**, *136*, 5332–5341.
- (10) Zhou, H.; Zhang, Z.; Jiang, C.; Guan, G.; Zhang, K.; Mei, Q.; Liu, R.; Wang, S. *Anal. Chem.* **2011**, *83*, 6913–6917.
- (11) Doering, W. E.; Nie, S. *Anal. Chem.* **2003**, *75*, 6171–6176.
- (12) Nie, S.; Emory, S. R. *Science* **1997**, *275*, 1102–1106.
- (13) Grajcar, L.; Baron, M. H. *J. Raman Spectrosc.* **2001**, *32*, 912–918.
- (14) Wang, Y.; Ji, W.; Sui, H.; Kitahama, Y.; Ruan, W.; Ozaki, Y.; Zhao, B. *J. Phys. Chem. C* **2014**, *118*, 10191–10197.
- (15) Wang, J.; Yang, L.; Liu, B.; Jiang, H.; Liu, R.; Yang, J.; Han, G.; Mei, Q.; Zhang, Z. *Anal. Chem.* **2014**, *86*, 3338–3345.
- (16) Zamaroni, V. M.; Timm, R. A.; Araki, K.; Toma, H. E. *Inorg. Chem.* **2008**, *47*, 2934–2936.
- (17) Wulff, G. *Angew. Chem., Int. Ed. Engl.* **1995**, *34*, 1812–1832.
- (18) Peng, Y.; Xie, Y.; Luo, J.; Nie, L.; Chen, Y.; Chen, L.; Du, S.; Zhang, Z. *Anal. Chim. Acta* **2010**, *674*, 190–200.
- (19) Xie, C.; Liu, B.; Wang, Z.; Gao, D.; Guan, G.; Zhang, Z. *Anal. Chem.* **2008**, *80*, 437–443.
- (20) Whitcombe, M. J.; Chianella, I.; Larcombe, L.; Piletsky, S. A.; Noble, J.; Porter, R.; Horgan, A. *Chem. Soc. Rev.* **2011**, *40*, 1547–1571.
- (21) Xie, C.; Zhang, Z.; Wang, D.; Guan, G.; Gao, D.; Liu, J. *Anal. Chem.* **2006**, *78*, 8339–8346.
- (22) Ouyang, R.; Lei, J.; Ju, H. *Chem. Commun.* **2008**, 5761–5763.
- (23) Liu, J.; Yang, K.; Deng, Q.; Li, Q.; Zhang, L.; Liang, Z.; Zhang, Y. *Chem. Commun.* **2011**, *47*, 3969–3971.
- (24) Gao, D.; Zhang, Z.; Wu, M.; Xie, C.; Guan, G.; Wang, D. *J. Am. Chem. Soc.* **2007**, *129*, 7859–7866.
- (25) Luo, J.; Zhang, L.; Chen, D.; Wang, P.; Zhao, J.; Peng, Y.; Du, S.; Zhang, Z. *Analyst* **2012**, *137*, 2891–2902.
- (26) Li, Y.; Yang, H. H.; You, Q. H.; Zhuang, Z. X.; Wang, X. R. *Anal. Chem.* **2006**, *78*, 317–320.
- (27) Friggeri, A.; Kobayashi, H.; Shinkai, S.; Reinhoudt, D. N. *Angew. Chem., Int. Ed.* **2001**, *40*, 4729–4731.
- (28) Roy, E.; Maity, S. K.; Patra, S.; Madhuri, R.; Sharma, P. K. *RSC Adv.* **2014**, *4*, 32881–32893.
- (29) Schirhagl, R.; Hall, E. W.; Fureder, I.; Zare, R. N. *Analyst* **2012**, *137*, 1495–1499.
- (30) Zhang, X.; Du, X.; Huang, X.; Lv, Z. *J. Am. Chem. Soc.* **2013**, *135*, 9248–9251.
- (31) Balamurugan, S.; Spivak, D. A. *J. Mol. Recognit.* **2011**, *24*, 915–929.
- (32) Batchelor, F. R.; Dewdney, J. M.; Gazzard, D. *Nature* **1965**, *206*, 362–364.
- (33) Ghebre-Sellassie, I.; Knevel, A. M.; Hem, S. L. *J. Pharm. Sci.* **1984**, *73*, 125–128.
- (34) García de Abajo, F. J. *Rev. Mod. Phys.* **2007**, *79*, 1267–1290.
- (35) Tiwari, V. S.; Anis, H. *J. Phys. Chem. C* **2011**, *115*, 1403–1409.
- (36) Kinnan, M. K.; Chumanov, G. *J. Phys. Chem. C* **2007**, *111*, 18010–18017.
- (37) Yu, D.; Yam, V. W. W. *J. Phys. Chem. B* **2005**, *109*, 5497–5503.
- (38) Sun, X.; Dong, S.; Wang, E. *J. Am. Chem. Soc.* **2005**, *127*, 13102–13103.